

IP-Adapter Is All You Need: Towards Fine-Tuning-Free Diffusion-Based Talking Face Generation

Hao Wu¹ Xiangyang Luo¹ Hao Wang² Jiawei Zhang³ Yi Zhang^{1,†} Jinwei Wang^{4,†}

¹Information Engineering University ²Huai'an University

³Chongqing University of Post and Telecommunications ⁴Nankai University

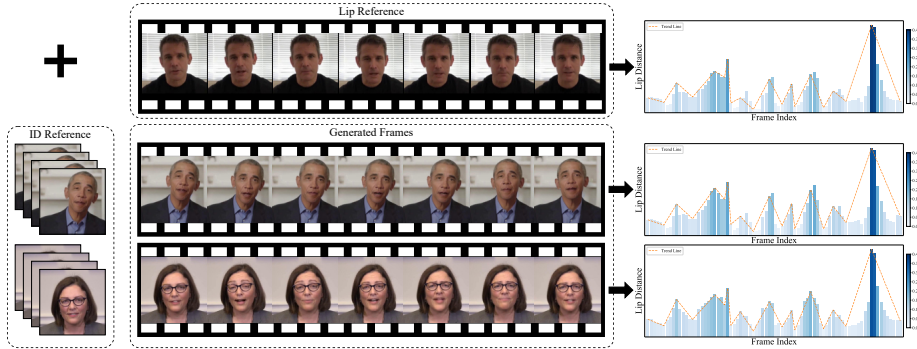


Figure 1. Visualization of videos generated by the proposed fine-tuning-free diffusion-based framework, FreeTalkDiff. The framework produces realistic, high-definition, lip-synced talking videos from lip and ID references. The accompanying lip-distance bar chart quantitatively illustrates the close alignment between the generated and reference lip motions, highlighting precise lip-control capability.

Abstract

With the rapid advancement of diffusion models, talking face generation has made remarkable progress. However, existing diffusion-based methods still require task-specific fine-tuning and large-scale audiovisual datasets, resulting in high computational costs that hinder scalability and accessibility of diffusion-based approaches across the research community. To address this, we propose a fine-tuning-free paradigm that directly performs talking face generation using the pretrained weights of Stable Diffusion and IP-Adapter. This backbone leverages the visual embedding capability of IP-Adapter to mine lip-related semantics from the pretrained Stable Diffusion. To address the challenges of identity drift, synchronization errors, and temporal instability, we also design three trainable-parameter-free components: 1) the Structurist, which explicitly disentangles and reassembles lip and appearance features to mitigate identity drift and appearance distortion; 2) the Structure Controller, which adaptively refines embeddings based on quasi-monotonic motion trends for precise lip synchronization; and 3) the Noise Sensor, which introduces






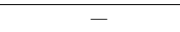

a Gaussian prior to detect and suppress flicker and jitter artifacts and enhance temporal consistency. Experimental results show that our method outperforms existing SOTA approaches in both lip-sync accuracy (at least 0.16 gain in PCLD) and visual fidelity (at least 0.7 improvement in FID), establishing a novel fine-tuning-free diffusion framework for talking face generation. The code is available at <https://github.com/tlemangen/FreeTalkDiff>.

1. Introduction

In recent years, talking face generation, which synthesizes talking videos of a target identity, has attracted widespread attention due to its vast application potential in areas such as entertainment [19, 51] and digital humans [26, 38]. With the rapid advancement of diffusion models [2, 16, 31, 36], their performance in image and video generation has significantly surpassed that of traditional generative adversarial networks [11, 12, 27, 29] and autoregressive models [6, 17, 33]. In particular, diffusion models demonstrate unique advantages in generation quality, and multimodal conditional control, making them a major driving force in advancing talking face generation.

[†]Corresponding authors. E-mail: tzyy4001@sina.com, wangjinwei@nankai.edu.cn

Table 1. Information for diffusion model-based methods. “#Params” indicates the number of parameters. “—” indicates no available data. “★” denotes the relative fine-tuning cost through a qualitative summary; more stars indicate higher cost.

Method	Affiliations	Trainable #Params	Train Sets	GPUs for Fine-tuning	Training Steps	Fine-tuning Cost
AniPortrait(arXiv’24) [40]		2.59B	HDTF [49], VFHQ [41], CelebV-HQ [52]	4 NVIDIA A100	—	★★★★★
Loopy(arXiv’24) [21]		—	Self-build, HDTF [49]	24 NVIDIA A100	—	★★★★★
MuseTalk(arXiv’24) [48]		0.85B	HDTF [49]	2 NVIDIA H20	300k	★★★★
LatentSync(arXiv’24) [23]		1.64B	VoxCeleb2 [8], HDTF [49]	—	—	★★★★
EchoMimic(AAAT’25) [5]		2.15B	Self-build, HDTF [49], CelebV-HQ [52]	8 NVIDIA A100	60k	★★★★★
Hallo2(ICLR’25) [9]		2.39B	Self-build, HDTF [49], CelebV-HQ [52]	8 NVIDIA A100	113k	★★★★★
Sonic(CVPR’25) [20]		1.65B	VFHQ [41], CelebV-Text [44], VoxCeleb2 [8]	—	—	★★★★
Ours	—	0.00 🟡	Not Required 🟡	Not Required 🟡	Not Required 🟡	Not Required 🟡

However, existing diffusion-based talking face generation methods require task-specific fine-tuning of diffusion models on large-scale audiovisual datasets. Given the massive parameter size and complex optimization of diffusion models, these methods often demand multiple high-performance GPUs and tens to hundreds of thousands of training steps, resulting in substantial computational and time costs. As shown in Tab. 1, existing diffusion-based methods typically involve fine-tuning models with billions of parameters. Representative examples include EchoMimic [5] and Hallo2 [9] were trained for 60k and 113k steps on eight A100, respectively, while Loopy [21] utilized as many as twenty-four A100 GPUs. This heavy dependence on computational resources and prolonged optimization greatly limits the scalability and accessibility of diffusion-based approaches across the research community.

To overcome the aforementioned bottleneck, this paper explores a novel framework: **performing talking face generation directly with a pretrained diffusion model, without any task-specific fine-tuning**. This approach eliminates the need for additional training, thereby significantly reducing computational and time costs. However, this framework introduces a key challenge: *how to mine lip-related knowledge from the vast knowledge of the pretrained diffusion model, thereby enabling controllable lip-sync generation?*

Our solution is motivated by an in-depth observation of pretrained model behaviors. We identify that the IP-Adapter [43], when paired with Stable Diffusion (SD) [31], naturally emphasizes lip-related features in facial representations, as the mouth region typically carries the main cues of the face. Therefore, we adopt a fine-tuning-free, controllable “SD + IP-Adapter” combination as our backbone for talking face generation. Building upon this backbone, we further propose three novel components with no trainable parameters: 1) **Structurist Module**: It explicitly disentangles redundant appearance features in the 3D face parameter space, preserving target lip motion information while effectively removing irrelevant factors such as color and texture, thereby mitigating identity drift and appearance distortion. 2) **Structure Controller**: It adaptively refines the embedding space based on the dynamic trends of ref-

erence lip movements, improving lip-control accuracy and synchronization. 3) **Noise Sensor**: It derives a Gaussian prior through hypothesis testing and formulaically models flicker and jitter noise patterns in generated videos. The noise patterns are mathematically proven, and the module integrates a spatially adaptive temporal filter to effectively suppress noise, thereby enhancing temporal consistency in video generation. Experimental results on the CREMA [4] and HDTF [49] datasets demonstrate that the “SD + IP-Adapter” backbone and these modules collectively improve both visual quality and lip synchronization, offering a novel fine-tuning-free framework for talking face generation.

In summary, our main contributions are as follows:

1. We propose a fine-tuning-free diffusion-based framework, FreeTalkDiff, for talking face generation. It is the first to directly leverage pretrained SD and IP-Adapter models, removing the need for costly fine-tuning on large datasets and greatly reducing resource overhead.
2. We design a 3DMM-based Structurist. This module disentangles and reassembles the useful lip and appearance features, thereby reinforcing identity preservation.
3. We propose an adaptive Structure Controller. By dynamically refining structure embeddings in accordance with the motion trends of reference lip movements, this module significantly improves the precision of lip control, achieving more natural and accurate lip synchronization.
4. We introduce a Gaussian-prior-based Noise Sensor, which formally models and detects flicker and jitter noise patterns in generated videos, and applies a spatially adaptive temporal filter to effectively enhance temporal consistency and realism.

2. Related work

2.1. Talking face generation

Early talking face generation methods primarily relied on GANs [11, 12, 27, 29] and autoregressive networks [6, 17, 33], which achieves notable progress in improving lip synchronization but suffers from limited vividness and naturalness. For example, Wav2Lip [28] introduces a pretrained SyncNet [7] discriminator to enforce audio-visual alignment. MakeItTalk [51] disentangles audio into content and

speaker style, and uses facial landmarks as intermediates. Audio2Head [39] enhances realism by predicting 6-DoF head poses and dense motion fields. Later methods such as TalkLip [37] and SadTalker [47] enhance articulation accuracy and 3D-awareness, but still suffer from blurry frames and coarse lip detail due to limited model capacity.

With the rise of diffusion models [2, 16, 31, 36], researchers have explored their potential in talking face generation. For instance, AniPortrait [40] combines 3D mesh prediction with diffusion rendering. Loopy [21] incorporates an inter- and intra-clip temporal module to capture long-term motion. MuseTalk [48] introduces selective information sampling and adaptive audio modulation to improve audio-visual alignment. More recent models, LatentSync [23], EchoMimic [5], and the Hallo family [9, 42], further advance temporal consistency, multimodal conditioning, and resolution. Sonic [20] further extend intra-clip audio perception to the global inter-clip level via motion-decoupled control and time-aware position shift fusion. Despite their advances, diffusion-based methods involve fine-tuning billion-scale parameters on large audiovisual datasets, demanding extensive GPU resources, as shown in Tab. 1. **This work aims to overcome this challenge by proposing a fine-tuning-free, highly synchronized, and high-fidelity solution for talking face generation.**

In addition, these methods can be divided into one-shot and few-shot paradigms based on the number of ID reference. One-shot methods rely on a single ID reference frame but often struggle with identity preservation, whereas few-shot methods leverage short reference videos to maintain personal dynamics and achieve higher fidelity. **Accordingly, our work focuses on the few-shot paradigm.**

2.2. IP-Adapter

In conditional diffusion-based generation, efficiently incorporating image prompts remains a key challenge. IP-Adapter [43] provides a solution by a CLIP Image Encoder [30] to extract a global image embedding (*i.e.*, **structure embedding**) and aligning it with the text-conditioned space through a lightweight adapter, enabling flexible control without modifying the SD backbone. Its variant, IP-Adapter-FaceID, further introduces identity embeddings from ArcFace [10] to enhance identity. These developments provide the technical foundation for using pretrained IP-Adapter to achieve fine-tuning-free talking face generation.

3. Motivation

The Motivation of the Backbone. Our goal is to achieve fine-tuning-free talking face generation to eliminate the heavy resource and time costs of training diffusion models. This leads to a key challenge: *How to mine and control the lip-related information from pretrained diffusion models?* To explore this question, we conduct an in-depth analysis of

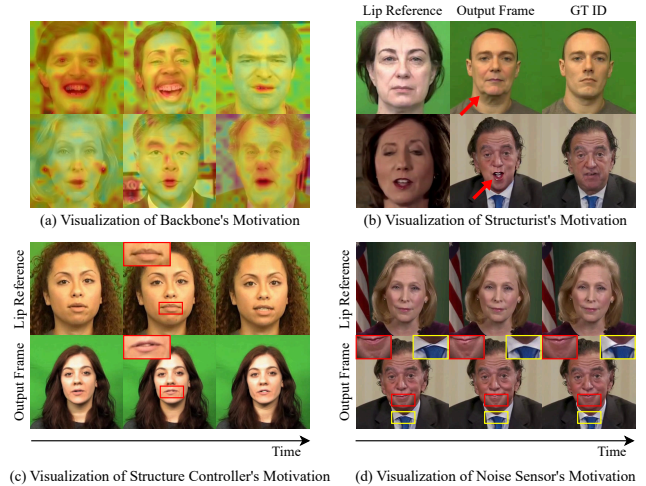


Figure 2. Visualization for motivations.

pretrained model characteristics. As shown in Fig. 2(a), we observed that structure embeddings in IP-Adapter exhibit strong attention to the mouth region, likely because its CLIP Image Encoder emphasizes semantic alignment between image regions and textual concepts, where the mouth often carries key semantic cues in face-related contexts [30, 50]. Motivated by this, we leverage IP-Adapter to inject lip cues from the target lip reference into its partner, SD. Consequently, we adopt the pretrained “SD + IP-Adapter” backbone for fine-tuning-free talking face generation.

The Motivation of the Structurist. As shown in Fig. 2(b), although IP-Adapter can achieve lip-sync control, directly feeding the lip reference introduces redundant texture and color, causing identity drift and appearance distortion. This leads to a key question: *How to remove redundant appearance information while preserving useful lip-related cues?* One possible approach is to explicitly disentangle lip-shape and appearance representations in the 3D face parameter space, allowing the system to retain useful lip-related information while removing interference from extraneous textures, thereby improving both lip-sync accuracy and identity consistency.

The Motivation of the Structure Controller. We further observe that IP-Adapter fail to capture subtle lip motion (Fig. 2(c)). This motivates another question: *How can the structure embedding be refined?* A feasible direction is to develop an adaptive refinement mechanism that adjusts the structure embedding according to the geometric properties of the embedding space, enabling to better track subtle lip dynamics and produce more precise lip synchronization.

The Motivation of the Noise Sensor. Finally, flicker and jitter artifacts often appear in generated mouth regions, as shown in Fig. 2(d), disrupting temporal smoothness. This raises the question: *How to suppress temporal noise to improve the visual stability?* A promising direction is to in-

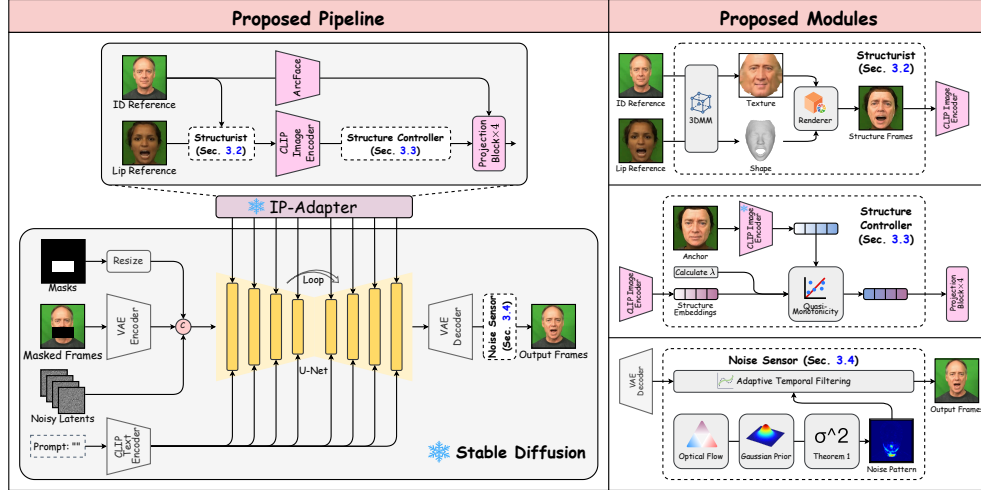


Figure 3. The pipeline of the proposed method.

roduce a noise-aware mechanism that models flicker and jitter over local motion variations, enabling spatially adaptive temporal filtering that selectively attenuates instability while preserving genuine lip movements, thereby improving both temporal consistency and overall visual fidelity.

4. Methodology

4.1. Pipeline overview

As shown in Fig. 3, our pipeline builds on the “image inpainting SD + IP-Adapter” backbone to support few-shot paradigm. Specifically, the encoded masked frames, random noise latents and scaled masks are first concatenated, and then passed into the denoising U-Net [32]. At each layer, we incorporate the FaceID version of the IP-Adapter to additionally inject identity embeddings. Each IP-Adapter layer receives the previous-layer latent, the text prompt, and two image prompts: identity and lip reference frames. The lip reference is first converted to structure frames via Structurist (Sec. 4.2), and then encoded by CLIP Image Encoder and refined by Structure Controller (Sec. 4.3) to capture structure embeddings with lip-shape and appearance cues, while the identity reference is processed by ArcFace [10] to enhance identity consistency. Finally, the fused embeddings are decoded into continuous talking frames via Noise Sensor (Sec. 4.4). **Notably, both SD and IP-Adapter are large-scale pretrained models, and our modules require no trainable parameters or fine-tuning, allowing direct application to talking face generation.**

4.2. 3DMM-based Structurist

In this section, we propose a 3DMM-based Structurist module to address the issue of redundant conditional information. As illustrated in Fig. 3, we first employ 3DMM [1, 18]

to project the lip reference faces into the shape and texture spaces, obtaining low-dimensional parameter representations that describe geometric structure and appearance attributes, respectively. Specifically, 3DMM represents the shape $P \in \mathbb{R}^{3n}$ and texture $Q \in \mathbb{R}^{3n}$ of any face as linear combinations of mean components and principal bases: $P = \bar{P} + \sum_{i=1}^M \alpha_i \sigma_i^P v_i^P$, $Q = \bar{Q} + \sum_{i=1}^M \beta_i \sigma_i^Q v_i^Q$, where α_i and β_i denote the shape and texture coefficients, respectively, and σ_i^P , σ_i^Q are the corresponding eigenvalues. The shape parameters capture lip-motion dynamics, while the texture parameters preserve color and detailed appearance information. Subsequently, to avoid interference from appearance, we combine the texture parameters of the target identity reference with the shape parameters of the lip reference, constructing a parametric representation that encapsulates the target appearance while retaining the desired lip-motion. Finally, using a renderer [22], this parametric representation is mapped to the image domain to generate a structure image prompt, referred to as the **structure frame**. This prompt is then fed into the CLIP Image Encoder of the IP-Adapter to obtain the structure embedding, which serves as the lip-motion condition for SD.

4.3. Quasi-monotonicity-based adaptive Structure Controller

To enhance the precision of lip-motion control, we introduce a quasi-monotonicity-based adaptive Structure Controller. We first analyze the mapping from structure embeddings to lip shapes and find two key properties in the structure embedding space \mathcal{E} .

Continuity and Quasi-Monotonicity. For each identity reference clip, we extract all structure embeddings and compute the Euclidean distances between upper and lower lip landmarks of generated frames as the corresponding *lip*

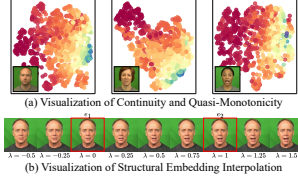


Figure 4. Visualization for Structure Controller.

distances. The high-dimensional embeddings are then reduced to a 2D manifold using Uniform Manifold Approximation and Projection [25] for visualization, and points are color-coded by lip distance—red for smaller lips and blue for larger ones. As shown in Fig. 4(a), two observations emerge: 1) **Continuity**: embeddings of the same identity form dense, smooth clusters, implying that \mathcal{E} is a continuous manifold. 2) **Quasi-Monotonicity**: color variations follow a clear directional gradient, showing that lip distance changes approximately monotonically along specific embedding directions. Formally, for any $e_1, e_2 \in \mathcal{E}$, the lip distance mapping $f : \mathcal{E} \rightarrow \mathbb{R}^+$ satisfies:

$$\begin{cases} f((1-\lambda)e_1 + \lambda e_2) \leq \min\{f(e_1), f(e_2)\} & \forall \lambda \in (-\infty, 0] \\ \min\{f(e_1), f(e_2)\} \leq f((1-\lambda)e_1 + \lambda e_2) \leq \max\{f(e_1), f(e_2)\} & \forall \lambda \in (0, 1) \\ f((1-\lambda)e_1 + \lambda e_2) \geq \max\{f(e_1), f(e_2)\} & \forall \lambda \in [1, +\infty) \end{cases} \quad (1)$$

This property implies that lip distance changes approximately monotonically along the interpolation direction, while extrapolation beyond this range yields overopened/closed lips (Fig. 4(b)).

Adaptive Adjustment. Leveraging the above findings, the Structure Controller dynamically adjusts structure embeddings according to the lip-motion trend of reference. Let S_{anchor} denote the structure frame with the smallest lip opening and $\gamma(\cdot)$ the lip-distance measurement. For the current frame S_{current} , the adjusted embedding is computed as:

$$e_{\text{current}} = (1-\lambda)\text{CLIP}(S_{\text{anchor}}) + \lambda\text{CLIP}(S_{\text{current}}), \quad (2)$$

where $\lambda = \frac{\gamma(L_{\text{current}})}{\gamma(L_{\text{previous}})}$, $\text{CLIP}(\cdot)$ denotes the CLIP Image Encoder, whose output corresponds to the structure embedding, and L_{current} and L_{previous} represent the current and previous lip reference frames, respectively. When $\gamma(L_{\text{current}}) > \gamma(L_{\text{previous}})$, the reference lips are opening, so $\lambda > 1$, causing e_{current} to extrapolate in the embedding space toward a more “open” direction according to Eq. (1), generating larger lips; conversely, when $\gamma(L_{\text{current}}) < \gamma(L_{\text{previous}})$, the reference lips are closing, so $\lambda < 1$, pulling e_{current} back toward the anchor, generating smaller lips. This adaptive adjustment mechanism leverages the quasi-monotonicity of the embedding space, allowing the generated lip shapes to be further corrected along the reference lip-motion trends, thereby compensat-

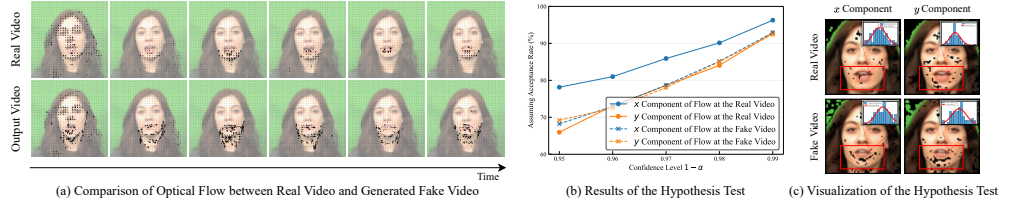


Figure 5. Visualization for Noise Sensor.

ing for discrepancies between the generated and reference lip shapes.

4.4. Gaussian-prior-based Noise Sensor

In this section, we propose a Gaussian-prior-based Noise Sensor to alleviate temporal continuity in generated videos.

Gaussian Prior and Hypothesis Testing. As shown in Fig. 5(a), the optical flow in the lip region of real videos exhibits smooth, continuous patterns, while that in generated videos often appears disordered and oscillatory due to jitter and flicker. To further analyze this discrepancy, we establish the following modeling hypothesis from a statistical distribution perspective.

Hypothesis 1. Let the optical flow vector of pixel (i, j) between two consecutive frames be \mathbf{V}_{ij} , which can be modeled as a 2D Gaussian distribution: $\mathbf{V}_{ij} \sim \mathcal{N}(\boldsymbol{\mu}_{ij}, \boldsymbol{\Sigma}_{ij})$, where the mean vector $\boldsymbol{\mu}_{ij} = (\mu_{\mathbf{V}_{ij,x}}, \mu_{\mathbf{V}_{ij,y}})^T$ represents the expected optical flow in the x and y directions, and $\boldsymbol{\Sigma}_{ij}$ is the covariance matrix describing the correlation between the two directions.

We validate this Gaussian hypothesis using the Shapiro-Wilk test [35] on lip-region optical flow sequences from both real and generated videos. As shown in Fig. 5(b), when the confidence level increases to 0.99, 92.4%–96.3% of pixels follow a Gaussian distribution. The fitted distributions in Fig. 5(c) further confirm that most optical flow components (*i.e.*, unmasked pixels) in the lip region can be well modeled by a Gaussian prior, validating its rationality.

Definition of Noise Pattern. Under the Gaussian assumption, we characterize the statistical properties of jitter and flicker noise in generated videos as follows:

Theorem 1. For pixel (i, j) , let $\mathbf{V}_{ij}^{\text{real}}$ and $\mathbf{V}_{ij}^{\text{fake}}$ denote the optical flow vectors in real and generated videos, respectively. The variance of the generated jitter and flicker noise $\hat{\mathbf{R}}_{ij}$ satisfies:

$$\sigma_{\hat{\mathbf{R}}_{ij}}^2 = \sigma_{\mathbf{V}_{ij}^{\text{fake}}}^2 - \frac{\text{Cov}^2(\mathbf{V}_{ij}^{\text{fake}}, \mathbf{V}_{ij}^{\text{real}})}{\sigma_{\mathbf{V}_{ij}^{\text{real}}}^2} \geq 0, \quad (3)$$

where $\sigma_{\mathbf{V}_{ij}^{\text{real}}}$, $\sigma_{\mathbf{V}_{ij}^{\text{fake}}}$ are the standard deviations of the optical flow vectors for the real and generated videos, respec-

Table 2. Quantitative comparison with existing talking face generation methods on the CREMA and HDTF datasets. “○” denotes one-shot setting, “●” denotes few-shot setting, “□” indicates non-diffusion-based methods, and “■” indicates diffusion-based methods.

Methods	Types	CREMA						HDTF					
		PD↓	CSLD↑	PCLD↑	FID↓	LPIPS↓	CPBD↑	PD↓	CSLD↑	PCLD↑	FID↓	LPIPS↓	CPBD↑
Wav2Lip(MM’20) [28]	●□	0.01950	0.649	0.235	14.9	0.056	0.134	0.01897	0.756	0.358	12.4	0.057	0.205
MakeItTalk(TOG’20) [51]	○□	0.02022	0.745	0.417	74.1	0.213	0.023	0.02443	0.752	0.250	87.5	0.293	0.042
Audio2Head(IJCAI’21) [39]	○□	0.01506	0.807	0.531	80.2	0.313	0.058	0.01794	0.760	0.282	92.2	0.314	0.058
TalkLip(CVPR’23) [37]	●□	0.01396	0.783	0.475	15.4	0.065	0.146	0.01736	0.805	0.424	14.0	0.060	0.201
SadTalker(CVPR’23) [47]	○□	0.02442	0.666	0.337	61.6	0.294	0.108	0.01652	0.816	0.544	35.2	0.225	0.212
MuseTalk(arXiv’24) [48]	●■	0.01853	0.668	0.313	5.2	0.037	0.143	0.01790	0.788	0.343	2.4	0.037	0.241
LatentSync(arXiv’24) [23]	●■	0.01767	0.762	0.429	2.2	0.032	0.189	0.01483	0.827	0.540	1.5	0.025	0.255
EchoMimic(AAAI’25) [5]	○■	0.01925	0.665	0.310	71.0	0.291	0.081	0.01596	0.840	0.524	50.1	0.476	0.145
Hallo2(ICLR’25) [9]	○■	0.02030	0.627	0.121	7.9	0.175	0.131	0.01524	0.844	0.547	3.9	0.191	0.211
Sonic(CVPR’25) [20]	○■	0.01774	0.707	0.408	32.9	0.228	0.104	0.01642	0.832	0.558	23.8	0.415	0.153
Ours	●■	0.00860	0.887	0.711	1.5	0.020	0.218	0.01026	0.883	0.718	0.5	0.023	0.289

tively. (The proof is detailed in Sec. 1 of Supplementary Material.)

A smaller noise variance indicates better temporal consistency between generated and real optical flow, while larger variance reflects more severe jitter and flicker. Accordingly, we define the **noise pattern** as: $D_{ij} = \|\sigma_{\hat{\mathbf{R}}_{ij}}\|_2 = \sqrt{\sigma_{\hat{\mathbf{R}}_{ij,x}}^2 + \sigma_{\hat{\mathbf{R}}_{ij,y}}^2}$, where higher D_{ij} values correspond to stronger jitter or flicker noise at the corresponding pixel location.

Adaptive Temporal Smoothness. To suppress flicker and jitter, we design a spatially adaptive temporal filter that adjusts its strength according to the estimated noise intensity. For each pixel (i, j) within a temporal window, the noise pattern D_{ij} serves as the standard deviation of a 1D Gaussian kernel, thus ensuring stronger smoothing in noisier regions. The kernel is $G_{ij}(k) = \text{softmax}(-\frac{k^2}{2D_{ij}^2})$, where k denotes the temporal offset from the current frame. This spatially varying design effectively mitigates flicker and enhances visual stability in generated videos.

5. Experiments and analysis

5.1. Experimental setup

Datasets. We evaluate our method on two widely used datasets: CREMA [4] (with green-screen backgrounds) and HDTF [49] (high-definition in-the-wild videos). All clips are standardized to 512×512 resolution, 25 fps, and 16 kHz audio sampling rate.

Baselines. We compare against ten representative methods covering GAN-based, autoregressive, and recent diffusion-based approaches: Wav2Lip [28], MakeItTalk [51], Audio2Head [39], TalkLip [37], SadTalker [47], MuseTalk [48], LatentSync [23], EchoMimic [5], Hallo2 [9], and Sonic [20].

Metrics. Lip-sync accuracy is evaluated using Procrustes Disparity (PD) [13], which removes rigid transformations to align 3D lip landmarks, and provides a robust

measure of geometric consistency. To assess the lip dynamic consistency, we use Cosine Similarity (CSLD) and Pearson Correlation (PCLD) of Lip Distance sequences. Visual quality is assessed via FID [15], LPIPS [46], and CPBD [3], measuring distribution distance, perceptual similarity, and clarity, respectively.

Implementation Details. Our framework builds upon Image Inpainting SD 1.5 [31] and IP-Adapter-FaceID [43]. We adopt the DPM-Solver++ scheduler [24] with 20 steps for efficient sampling. The Noise Sensor employs an adaptive Gaussian temporal filter with a kernel size of 5. Text prompts are left empty to avoid semantic interference.

5.2. Comparative experiments

5.2.1. Quantitative comparison

This section reports quantitative comparisons with ten representative talking face generation methods on the CREMA and HDTF datasets, as shown in Tab. 2.

In terms of lip-sync performance, our method achieves the lowest PD (CREMA: 0.00860, HDTF: 0.01026), indicating strong geometric consistency between generated and the ground-truth lips. For CSLD and PCLD, which measure temporal consistency and correlation of lip motion, our method also achieves the best results (CREMA: 0.887/0.711, HDTF: 0.883/0.718). These improvements primarily benefit from the adaptive Structure Controller, which dynamically refines structure embeddings for aligned lip motion. Moreover, the fine-tuning-free backbone ensures robust generalization across datasets by leveraging large-scale pretraining on LAION dataset [34].

Regarding visual quality, our method also surpasses all baselines, achieving FID/LPIPS of 1.5/0.020 on CREMA and 0.5/0.023 on HDTF. Meanwhile, our method achieves the highest CPBD values for image clarity (CREMA: 0.218, HDTF: 0.289), indicating that generated images are closer to real videos in terms of detail. This improvement results from the Structurist’s disentanglement mechanism that maintains appearance, and the Noise Sensor, which effec-



Figure 6. Visualization of generated frames. Blue, orange, and red boxes denote correct, weak, and opposite lip-motion trends relative to the ground-truth reference frames, respectively.

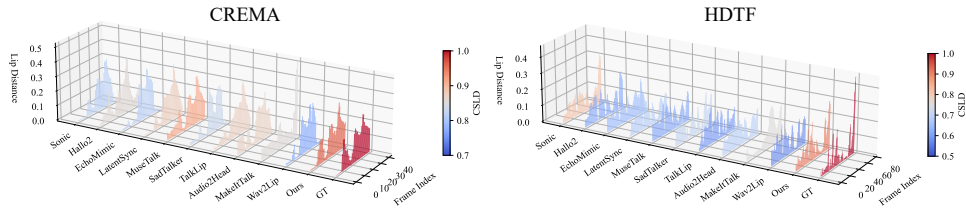


Figure 7. Visualization of lip distance. Redder indicates higher CSLD, bluer indicates lower CSLD.

tively suppresses flicker and jitter. Notably, few-shot methods generally produce higher visual quality than one-shot methods due to the preservation of the unmasked area. Our method further extends this advantage by enhancing the realism of the mouth area.

5.2.2. Qualitative comparison

Visualization of Generated Frames. To intuitively evaluate the lip-sync performance of our method, we compare its generated frames with those from multiple baseline methods on the CREMA and HDTF datasets. Specifically, we display two consecutive generated frames alongside their corresponding ground-truth lip reference frames, as shown

in Fig. 6. The results show that subtle or opposite lip movement trends are common among baseline methods, reflecting their limitations in lip-motion-driven modeling. In contrast, our method produces lip movements consistent with the ground-truth reference frames, avoiding incorrect directions or lack of motion, thereby achieving significant advantages in lip-sync accuracy.

Visualization of Lip Distance. To provide a more intuitive visualization of our method’s effectiveness in lip-sync, we compare the lip distance sequences generated by our method with those of multiple baseline methods. Specifically, we select examples in Fig. 6 and plot the ground-truth



Figure 8. Visualization ablation results for Structurist.

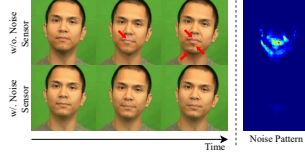


Figure 12. Visualization ablation results for Noise Sensor.

lip distance sequences along with the sequences generated by each method. As shown in Fig. 7, our method’s lip distance sequences closely match the ground-truth, accurately capturing the amplitude and rhythm of lip opening and closing, thereby achieving the highest CSLD scores among all methods. In contrast, baseline methods exhibit noticeable deviations in lip opening and closing rhythms, resulting in varying degrees of distortion in lip movements.

5.3. Ablation study

Effectiveness of Structurist. Fig. 8 shows that without the Structurist, redundant texture and color from the structure frame leak into the output, causing identity drift and appearance distortion. Incorporating Structurist effectively suppresses such leakage, yielding results consistent with the GT ID. Additionally, since texture information incorporates expression information, Structurist is also capable of effectively preserving the mouth expressions of GT ID. These results validate the role of Structurist in effectively disentangling lip motion information from appearance features.

Effectiveness of Structure Controller. As shown in Fig. 9, removing Structure Controller (w/o.) leads to larger deviations between the generated and reference lip shapes. Introducing it (w/.) significantly reduces PD and improves CSLD and PCLD, indicating better alignment in both amplitude and dynamics. The visualization in Fig. 10 further confirms that the controller enables the generated lips to more accurately follow the reference (GT Lip), demonstrating its importance in adaptively correcting lip motion trends and enhancing lip-sync accuracy.

Effectiveness of Noise Sensor. As shown in Fig. 11, removing Noise Sensor (w/o.) leads to notably higher FVD and MNP (*i.e.*, Mean of Noise Pattern) values, indicating degraded temporal smoothness. In contrast, incorporating it (w/.) significantly reduces both metrics, confirming its role in enhancing temporal coherence. Fig. 12 further shows

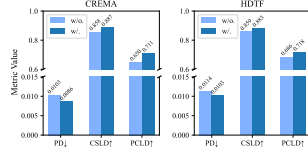


Figure 9. Quantitative ablation results for Structure Controller.

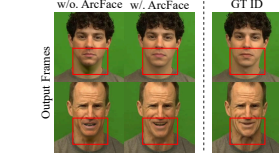


Figure 13. Visualization ablation results for ArcFace.

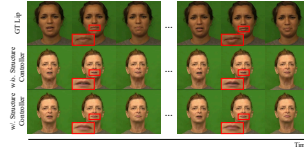


Figure 10. Visualization ablation for Structure Controller.

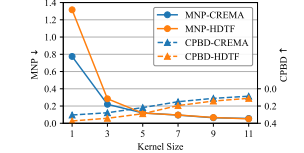


Figure 14. Quantitative ablation results for kernel size.

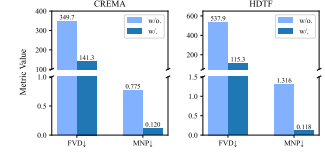


Figure 11. Quantitative ablation results for Noise Sensor.

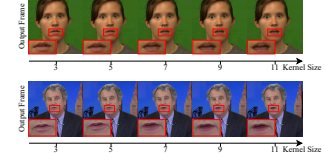


Figure 15. Visualization results with different kernel sizes.

that the Noise Sensor effectively suppresses mouth-region flickering and jittering (red arrows), yielding smoother and more stable video dynamics.

Effectiveness of ArcFace. Without ArcFace, the IP-Adapter degenerates from the FaceID version to the base version. As shown in Fig. 13, the generated mouth region exhibits noticeable color and jawline discrepancies compared to the ground-truth identity face, resulting in a loss of identity information. In contrast, with ArcFace, the generated mouth region closely matches the real face. Visualization results demonstrate that incorporating ArcFace enhances identity preservation.

Comparison between Different Kernel Sizes. As shown in Fig. 14, larger kernels effectively reduce flicker noise (lower MNP) but cause motion blur (lower CPBD). Visual results in Fig. 15 confirm that excessive kernel sizes lead to mouth-region blurring and ghosting. Overall, a kernel size of 5 offers the best trade-off between temporal smoothness and visual clarity.

6. Conclusion and future work

This paper introduces a fine-tuning-free diffusion-based framework, FreeTalkDiff, for talking face generation, integrating the Structurist, Structure Controller, and Noise Sensor modules to enhance identity consistency, lip synchronization, and temporal smoothness. Experimental results have demonstrated superior lip-sync accuracy and visual quality on multiple datasets, validating the potential of pretrained diffusion models for high-fidelity talking face synthesis without fine-tuning. In future work, we plan to 1) explore multimodal fusion strategies that jointly model semantic, emotional, and expressive cues to enhance naturalness and expressiveness; and 2) integrate large language models with visual diffusion models to develop end-to-end parameter-frozen audiovisual generation systems, offering a new framework for multimodal digital human synthesis.

7. Acknowledgments

This work is supported by the Natural Science Foundation for Excellent Young Scholars of Henan Province (Grants No. 252300421233), the National Natural Science Foundation of China (Grants No. U23A20305, 62472229, U24B20179), the Innovation Scientists and Technicians Troop Construction Projects of Henan Province (Grants No. 254000510007), and the Research Project of Quan Cheng Laboratory (Grants No. QCL20250203).

References

- [1] Volker Blanz and Thomas Vetter. A morphable model for the synthesis of 3d faces. In *Seminal Graphics Papers: Pushing the Boundaries, Volume 2*, pages 157–164. 2023. 4
- [2] Andreas Blattmann, Tim Dockhorn, Sumith Kulal, Daniel Mendelevitch, Maciej Kilian, Dominik Lorenz, Yam Levi, Zion English, Vikram Voleti, Adam Letts, et al. Stable video diffusion: Scaling latent video diffusion models to large datasets. *arXiv preprint arXiv:2311.15127*, 2023. 1, 3
- [3] P Bohr, Rupali Gargote, Rupali Vhorkate, RU Yawle, and VK Bairagi. A no reference image blur detection using cumulative probability blur detection (cpbd) metric. *International Journal of Science and Modern Engineering*, 1(5), 2013. 6
- [4] Houwei Cao, David G Cooper, Michael K Keutmann, Ruben C Gur, Ani Nenkova, and Ragini Verma. Crema-d: Crowd-sourced emotional multimodal actors dataset. *IEEE transactions on affective computing*, 5(4):377–390, 2014. 2, 6
- [5] Zhiyuan Chen, Jiajiong Cao, Zhiquan Chen, Yuming Li, and Chenguang Ma. Echomimic: Lifelike audio-driven portrait animations through editable landmark conditions. In *Proceedings of the AAAI Conference on Artificial Intelligence*, pages 2403–2410, 2025. 2, 3, 6
- [6] Junyoung Chung, Caglar Gulcehre, KyungHyun Cho, and Yoshua Bengio. Empirical evaluation of gated recurrent neural networks on sequence modeling. *arXiv preprint arXiv:1412.3555*, 2014. 1, 2
- [7] Joon Son Chung and Andrew Zisserman. Out of time: automated lip sync in the wild. In *Asian conference on computer vision*, pages 251–263. Springer, 2016. 2
- [8] Joon Son Chung, Arsha Nagrani, and Andrew Zisserman. Voxceleb2: Deep speaker recognition. *arXiv preprint arXiv:1806.05622*, 2018. 2, 3, 6
- [9] Jiahao Cui, Hui Li, Yao Yao, Hao Zhu, Hanlin Shang, Kaihui Cheng, Hang Zhou, Siyu Zhu, and Jingdong Wang. Hallo2: Long-duration and high-resolution audio-driven portrait image animation. In *The Thirteenth International Conference on Learning Representations*, 2025. 2, 3, 6
- [10] Jiankang Deng, Jia Guo, Niannan Xue, and Stefanos Zafeiriou. Arcface: Additive angular margin loss for deep face recognition. In *Proceedings of the IEEE/CVF conference on computer vision and pattern recognition*, pages 4690–4699, 2019. 3, 4
- [11] Ian Goodfellow, Jean Pouget-Abadie, Mehdi Mirza, Bing Xu, David Warde-Farley, Sherjil Ozair, Aaron Courville, and Yoshua Bengio. Generative adversarial networks. *Communications of the ACM*, 63(11):139–144, 2020. 1, 2
- [12] Ian J Goodfellow, Jean Pouget-Abadie, Mehdi Mirza, Bing Xu, David Warde-Farley, Sherjil Ozair, Aaron Courville, and Yoshua Bengio. Generative adversarial nets. *Advances in neural information processing systems*, 27, 2014. 1, 2
- [13] John C Gower. Generalized procrustes analysis. *Psychometrika*, 40(1):33–51, 1975. 6
- [14] Yuwei Guo, Ceyuan Yang, Anyi Rao, Zhengyang Liang, Yaohui Wang, Yu Qiao, Maneesh Agrawala, Dahua Lin, and Bo Dai. Animatediff: Animate your personalized text-to-image diffusion models without specific tuning. In *The Twelfth International Conference on Learning Representations*, 2024. 2
- [15] Martin Heusel, Hubert Ramsauer, Thomas Unterthiner, Bernhard Nessler, and Sepp Hochreiter. Gans trained by a two time-scale update rule converge to a local nash equilibrium. *Advances in neural information processing systems*, 30, 2017. 6
- [16] Jonathan Ho, Ajay Jain, and Pieter Abbeel. Denoising diffusion probabilistic models. *Advances in neural information processing systems*, 33:6840–6851, 2020. 1, 3
- [17] Sepp Hochreiter and Jürgen Schmidhuber. Long short-term memory. *Neural computation*, 9(8):1735–1780, 1997. 1, 2
- [18] Patrik Huber, Guosheng Hu, Rafael Tena, Pouria Mortazavian, Willem P Koppen, William Christmas, Matthias Rätzsch, and Josef Kittler. A multiresolution 3d morphable face model and fitting framework. In *Proceedings of the 11th joint conference on computer vision, imaging and computer graphics theory and applications*, pages 79–86. SciTePress, 2016. 4
- [19] Xinya Ji, Hang Zhou, Kaisiyuan Wang, Qianyi Wu, Wayne Wu, Feng Xu, and Xun Cao. Eamm: One-shot emotional talking face via audio-based emotion-aware motion model. In *ACM SIGGRAPH 2022 conference proceedings*, pages 1–10, 2022. 1
- [20] Xiaozhong Ji, Xiaobin Hu, Zhihong Xu, Junwei Zhu, Chuming Lin, Qingdong He, Jiangning Zhang, Donghao Luo, Yi Chen, Qin Lin, et al. Sonic: Shifting focus to global audio perception in portrait animation. In *Proceedings of the Computer Vision and Pattern Recognition Conference*, pages 193–203, 2025. 2, 3, 6
- [21] Jianwen Jiang, Chao Liang, Jiaqi Yang, Gaojie Lin, Tianyun Zhong, and Yanbo Zheng. Loopy: Taming audio-driven portrait avatar with long-term motion dependency. *arXiv preprint arXiv:2409.02634*, 2024. 2, 3
- [22] Samuli Laine, Janne Hellsten, Tero Karras, Yeongho Seol, Jaakko Lehtinen, and Timo Aila. Modular primitives for high-performance differentiable rendering. *ACM Transactions on Graphics (ToG)*, 39(6):1–14, 2020. 4
- [23] Chunyu Li, Chao Zhang, Weikai Xu, Jingyu Lin, Jinghui Xie, Weiguo Feng, Bingyue Peng, Cunjian Chen, and Weiwei Xing. Latentsync: Taming audio-conditioned latent diffusion models for lip sync with syncnet supervision. *arXiv preprint arXiv:2412.09262*, 2024. 2, 3, 6
- [24] Cheng Lu, Yuhao Zhou, Fan Bao, Jianfei Chen, Chongxuan Li, and Jun Zhu. Dpm-solver++: Fast solver for guided sam-

- pling of diffusion probabilistic models. *Machine Intelligence Research*, pages 1–22, 2025. 6
- [25] Leland McInnes, John Healy, Nathaniel Saul, and Lukas Großberger. Umap: Uniform manifold approximation and projection. *Journal of Open Source Software*, 3(29):861, 2018. 5
- [26] Rang Meng, Xingyu Zhang, Yuming Li, and Chenguang Ma. Echomimicv2: Towards striking, simplified, and semi-body human animation. In *Proceedings of the Computer Vision and Pattern Recognition Conference*, pages 5489–5498, 2025. 1
- [27] Mehdi Mirza and Simon Osindero. Conditional generative adversarial nets. *arXiv preprint arXiv:1411.1784*, 2014. 1, 2
- [28] KR Prajwal, Rudrabha Mukhopadhyay, Vinay P Namboodiri, and CV Jawahar. A lip sync expert is all you need for speech to lip generation in the wild. In *Proceedings of the 28th ACM international conference on multimedia*, pages 484–492, 2020. 2, 6
- [29] Alec Radford, Luke Metz, and Soumith Chintala. Un-supervised representation learning with deep convolutional generative adversarial networks. *arXiv preprint arXiv:1511.06434*, 2015. 1, 2
- [30] Alec Radford, Jong Wook Kim, Chris Hallacy, Aditya Ramesh, Gabriel Goh, Sandhini Agarwal, Girish Sastry, Amanda Askell, Pamela Mishkin, Jack Clark, et al. Learning transferable visual models from natural language supervision. In *International conference on machine learning*, pages 8748–8763. PmLR, 2021. 3
- [31] Robin Rombach, Andreas Blattmann, Dominik Lorenz, Patrick Esser, and Björn Ommer. High-resolution image synthesis with latent diffusion models. In *Proceedings of the IEEE/CVF conference on computer vision and pattern recognition*, pages 10684–10695, 2022. 1, 2, 3, 6
- [32] Olaf Ronneberger, Philipp Fischer, and Thomas Brox. U-net: Convolutional networks for biomedical image segmentation. In *International Conference on Medical image computing and computer-assisted intervention*, pages 234–241. Springer, 2015. 4
- [33] Haşim Sak, Andrew Senior, and Françoise Beaufays. Long short-term memory based recurrent neural network architectures for large vocabulary speech recognition. *arXiv preprint arXiv:1402.1128*, 2014. 1, 2
- [34] Christoph Schuhmann, Romain Beaumont, Richard Vencu, Cade Gordon, Ross Wightman, Mehdi Cherti, Theo Coombes, Aarush Katta, Clayton Mullis, Mitchell Wortsman, et al. Laion-5b: An open large-scale dataset for training next generation image-text models. *Advances in neural information processing systems*, 35:25278–25294, 2022. 6
- [35] S Shaphiro and MJB Wilk. An analysis of variance test for normality. *Biometrika*, 52(3):591–611, 1965. 5
- [36] Jiaming Song, Chenlin Meng, and Stefano Ermon. Denoising diffusion implicit models. *arXiv preprint arXiv:2010.02502*, 2020. 1, 3
- [37] Jiadong Wang, Xinyuan Qian, Malu Zhang, Robby T Tan, and Haizhou Li. Seeing what you said: Talking face generation guided by a lip reading expert. In *Proceedings of the IEEE/CVF Conference on Computer Vision and Pattern Recognition*, pages 14653–14662, 2023. 3, 6
- [38] Mengchao Wang, Qiang Wang, Fan Jiang, Yaqi Fan, Yunpeng Zhang, Yonggang Qi, Kun Zhao, and Mu Xu. Fantasytalking: Realistic talking portrait generation via coherent motion synthesis. *arXiv preprint arXiv:2504.04842*, 2025. 1
- [39] S Wang, L Li, Y Ding, C Fan, and X Yu. Audio2head: Audio-driven one-shot talking-head generation with natural head motion. In *IJCAI International Joint Conference on Artificial Intelligence*, pages 1098–1105, 2021. 3, 6
- [40] Huawei Wei, Zejun Yang, and Zhisheng Wang. Aniportrait: Audio-driven synthesis of photorealistic portrait animation. *arXiv preprint arXiv:2403.17694*, 2024. 2, 3
- [41] Liangbin Xie, Xintao Wang, Honglun Zhang, Chao Dong, and Ying Shan. Vfhq: A high-quality dataset and benchmark for video face super-resolution. In *Proceedings of the IEEE/CVF Conference on Computer Vision and Pattern Recognition*, pages 657–666, 2022. 2
- [42] Mingwang Xu, Hui Li, Qingkun Su, Hanlin Shang, Liwei Zhang, Ce Liu, Jingdong Wang, Yao Yao, and Siyu Zhu. Hallo: Hierarchical audio-driven visual synthesis for portrait image animation. *arXiv preprint arXiv:2406.08801*, 2024. 3
- [43] Hu Ye, Jun Zhang, Sibio Liu, Xiao Han, and Wei Yang. Ip-adapt: Text compatible image prompt adapter for text-to-image diffusion models. *arXiv preprint arXiv:2308.06721*, 2023. 2, 3, 6
- [44] Jianhui Yu, Hao Zhu, Liming Jiang, Chen Change Loy, Weidong Cai, and Wayne Wu. Celebv-text: A large-scale facial text-video dataset. In *Proceedings of the IEEE/CVF Conference on Computer Vision and Pattern Recognition*, pages 14805–14814, 2023. 2
- [45] Lvmin Zhang, Anyi Rao, and Maneesh Agrawala. Adding conditional control to text-to-image diffusion models. In *Proceedings of the IEEE/CVF international conference on computer vision*, pages 3836–3847, 2023. 3
- [46] Richard Zhang, Phillip Isola, Alexei A Efros, Eli Shechtman, and Oliver Wang. The unreasonable effectiveness of deep features as a perceptual metric. In *Proceedings of the IEEE conference on computer vision and pattern recognition*, pages 586–595, 2018. 6
- [47] Wenxuan Zhang, Xiaodong Cun, Xuan Wang, Yong Zhang, Xi Shen, Yu Guo, Ying Shan, and Fei Wang. Sadtalker: Learning realistic 3d motion coefficients for stylized audio-driven single image talking face animation. In *Proceedings of the IEEE/CVF conference on computer vision and pattern recognition*, pages 8652–8661, 2023. 3, 6
- [48] Yue Zhang, LIU Minhao, Zhaokang Chen, Bin Wu, Chao Zhan, Yingjie He, JUNXIN HUANG, Wenjiang Zhou, et al. Musetalk: Real-time high quality lip synchronization with latent space inpainting. 2024. 2, 3, 6
- [49] Zhimeng Zhang, Lincheng Li, Yu Ding, and Changjie Fan. Flow-guided one-shot talking face generation with a high-resolution audio-visual dataset. In *Proceedings of the IEEE/CVF conference on computer vision and pattern recognition*, pages 3661–3670, 2021. 2, 6
- [50] Ya Zhao, Rui Xu, Xinchao Wang, Peng Hou, Haihong Tang, and Mingli Song. Hearing lips: Improving lip reading by distilling speech recognizers. In *Proceedings of the AAAI Conference on Artificial Intelligence*, pages 6917–6924, 2020. 3

- [51] Yang Zhou, Xintong Han, Eli Shechtman, Jose Echevarria, Evangelos Kalogerakis, and Dingzeyu Li. Makeltalk: speaker-aware talking-head animation. *ACM Transactions On Graphics (TOG)*, 39(6):1–15, 2020. [1](#), [2](#), [6](#)
- [52] Hao Zhu, Wayne Wu, Wentao Zhu, Liming Jiang, Siwei Tang, Li Zhang, Ziwei Liu, and Chen Change Loy. Celebv-hq: A large-scale video facial attributes dataset. In *European conference on computer vision*, pages 650–667. Springer, 2022. [2](#)

IP-Adapter Is All You Need: Towards Fine-Tuning-Free Diffusion-Based Talking Face Generation

Supplementary Material

1. The proof of Theorem 1

This section provides a detailed proof of Theorem 1, aiming to rigorously justify the theoretical claims presented in the main paper. All derivations and intermediate steps are included to ensure completeness and clarity.

Taking the x -direction component of the random variable \mathbf{V}_{ij} as an example, we define it as a new random variable X . The optical flow component in the x direction of the real video is denoted by X^{real} , that of the generated video by X^{fake} , the ideal flicker-free and jitter-free version by Z , and the noise that causes flicker and jitter by R . Therefore, according to the Gaussian prior, these random variables satisfy

$$X^{real} \sim \mathcal{N}(\mu_{X^{real}}, \sigma_{X^{real}}^2), \quad (1)$$

$$X^{fake} = Z + R \sim \mathcal{N}(\mu_{X^{fake}}, \sigma_{X^{fake}}^2), \quad (2)$$

Since the distributions of Z and R are unknown, we aim to approximate the ideal flicker-free motion pattern Z using a Gaussian random variable \hat{Z} according to the Gaussian prior. Assuming that the desired motion pattern should be consistent with the real one, \hat{Z} can be derived from X^{real} through a linear transformation with parameters α and β :

$$\hat{Z} = \alpha X^{real} + \beta \sim \mathcal{N}(\alpha \mu_{X^{real}} + \beta, \alpha^2 \sigma_{X^{real}}^2). \quad (3)$$

We derive the optimal estimation of \hat{Z} through the following lemma.

Lemma 1. *To minimize the estimation error $\mathbb{E}[(Z - \hat{Z})^2]$, the optimal parameters α and β are given by*

$$\begin{cases} \alpha^* = \frac{\text{Cov}(Z, X^{real})}{\sigma_{X^{real}}^2} \\ \beta^* = \mu_Z - \frac{\text{Cov}(Z, X^{real})}{\sigma_{X^{real}}^2} \mu_{X^{real}} \end{cases}. \quad (4)$$

Consequently, the optimal estimation \hat{Z}^* can be expressed as

$$\hat{Z}^* = \frac{\text{Cov}(Z, X^{real})}{\sigma_{X^{real}}^2} (X^{real} - \mu_{X^{real}}) + \mu_Z. \quad (5)$$

Proof. To derive the optimal estimation of \hat{Z} , we define the estimation error as

$$J(\alpha, \beta) = \mathbb{E}[(Z - \hat{Z})^2] = \mathbb{E}[(Z - (\alpha X^{real} + \beta))^2]. \quad (6)$$

To minimize the estimation error, the first-order derivatives with respect to α and β must vanish:

$$\begin{cases} \frac{\partial J}{\partial \alpha} = -2\mathbb{E}[(Z - (\alpha X^{real} + \beta))X^{real}] = 0, \\ \frac{\partial J}{\partial \beta} = -2\mathbb{E}[Z - (\alpha X^{real} + \beta)] = 0. \end{cases} \quad (7)$$

Solving the above equations yields the optimal parameters:

$$\begin{cases} \alpha^* = \frac{\text{Cov}(Z, X^{real})}{\sigma_{X^{real}}^2}, \\ \beta^* = \mu_Z - \frac{\text{Cov}(Z, X^{real})}{\sigma_{X^{real}}^2} \mu_{X^{real}}. \end{cases} \quad (8)$$

Substituting these parameters into $\hat{Z} = \alpha X^{real} + \beta$ gives the optimal estimation:

$$\hat{Z}^* = \frac{\text{Cov}(Z, X^{real})}{\sigma_{X^{real}}^2} (X^{real} - \mu_{X^{real}}) + \mu_Z. \quad (9)$$

This result indicates that the optimal estimation \hat{Z}^* can be interpreted as a linear regression prediction of the real optical flow distribution X^{real} , where the regression coefficient is governed by the covariance relationship between the ideal motion pattern Z and the real one X^{real} . \square

Based on the optimal estimation \hat{Z}^* derived in Lemma 1, the estimated noise component can be expressed as

$$\hat{R} = X^{fake} - \hat{Z}^*. \quad (10)$$

Assuming that flicker and jitter are induced by the inherent diffusion noise, *i.e.*, R is statistically independent of the other random variables, the variance of the estimated noise can be written as

$$\sigma_{\hat{R}}^2 = \text{Var}(X^{fake} - \hat{Z}^*) \quad (11)$$

$$= \sigma_{X^{fake}}^2 + \sigma_{\hat{Z}^*}^2 - 2\text{Cov}(X^{fake}, \hat{Z}^*) \quad (12)$$

$$= \sigma_{X^{fake}}^2 + \frac{\text{Cov}^2(Z, X^{real})}{\sigma_{X^{real}}^2} \quad (13)$$

$$- 2 \frac{\text{Cov}(Z, X^{real})}{\sigma_{X^{real}}^2} \text{Cov}(X^{fake}, X^{real}) \quad (14)$$

$$= \sigma_{X^{fake}}^2 + \frac{(\text{Cov}(X^{fake}, X^{real}) - \text{Cov}(R, X^{real}))^2}{\sigma_{X^{real}}^2} \quad (15)$$

$$- 2 \frac{\text{Cov}(X^{fake}, X^{real}) - \text{Cov}(R, X^{real})}{\sigma_{X^{real}}^2} \text{Cov}(X^{fake}, X^{real}) \quad (16)$$

$$= \sigma_{X^{fake}}^2 - \frac{\text{Cov}^2(X^{fake}, X^{real})}{\sigma_{X^{real}}^2}. \quad (17)$$



Figure 1. Visualization of mouth expression controlled by the text prompt.

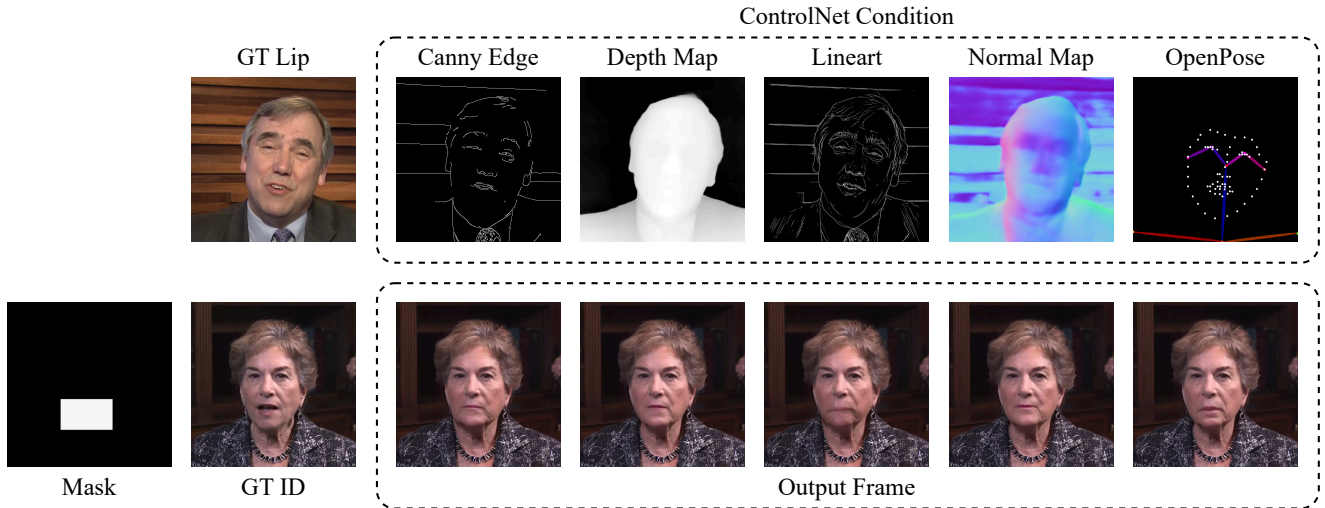


Figure 2. Visualization of lip control using different ControlNet conditions.

The result shows that the noise variance depends on the covariance between the generated and real optical flows. The non-negativity of this variance is guaranteed by the Cauchy–Schwarz inequality:

$$\sigma_R^2 = \sigma_{X^{fake}}^2 - \frac{\text{Cov}^2(X^{fake}, X^{real})}{\sigma_{X^{real}}^2} \quad (18)$$

$$\geq \sigma_{X^{fake}}^2 - \frac{\sigma_{X^{fake}}^2 \sigma_{X^{real}}^2}{\sigma_{X^{real}}^2} \quad (19)$$

$$= 0. \quad (20)$$

Similarly, the same result holds for the y -direction component of the random variable \mathbf{V}_{ij} .

2. Discussion

In this section, we discuss several key aspects of our work. We first explore the controllability of mouth expressions under few-shot settings, then examine the potential development of AnimateDiff and IP-Adapter communities as a backbone for fine-tuning-free talking face generation, and

finally analyze the effectiveness of pretrained ControlNet for lip control.

Controllable Mouth Expression. In the few-shot setting, the generated mouth region typically retains the original expression. As demonstrated in the ablation study of the Structurist, the mouth expression primarily originates from the texture information of the structural frame and effectively preserves the expression features of the identity reference. As a functional extension, we further explore the ability to control mouth expressions via text prompts. As shown in Fig. 1, when expression-related semantics are injected into the generated frames through the text prompts, the mouth region responds accordingly, demonstrating a certain level of controllability. However, such text-prompt-based expression modification may sometimes cause inconsistencies with other facial regions, leading to a slightly unnatural appearance.

Development of AnimateDiff and IP-Adapter Communities. AnimateDiff [14] extends SD 1.5 by introducing pluggable motion modules and motion LoRA, enabling coherent video generation. This design does not compromise



Figure 3. Visualization of the visible watermark.

the compatibility with IP-Adapter, which also operates as a plugin within the SD 1.5 framework. Consequently, AnimateDiff can be paired with IP-Adapter to form a *seemingly* feasible fine-tuning-free backbone for talking face generation. However, the current IP-Adapter only provides a shared lip reference for the entire input video clip, rather than assigning distinct lip features to each frame. This limitation causes the “AnimateDiff + IP-Adapter” backbone to produce static lip shape across frames, preventing it from achieving fine-tuning-free talking face generation. Looking ahead, with the continued evolution of the AnimateDiff and IP-Adapter communities and the increasing modularity and openness of these frameworks, we believe this combined backbone holds great potential to advance fine-tuning-free talking face generation.

Analysis of Pretrained ControlNet for Lip Control.

To investigate whether pretrained ControlNet [45] can effectively control lip generation, we conduct conditional generation experiments using various types of ControlNet inputs, including Canny edge, depth map, lineart, normal map, and OpenPose. As shown in Fig. 2, the generated results reveal that pretrained ControlNet fails to accurately control mouth shapes. This limitation may stem from two main factors: 1) many ControlNet conditions (*e.g.*, Canny edge, depth map, and normal map) tend to destroy lip-related details, and 2) the internal representations of ControlNet are generally not designed to capture fine-grained lip cues—although OpenPose provides mouth landmarks, its pretrained model focuses more on global posture rather than localized mouth dynamics. These findings indicate that pretrained ControlNet lacks explicit sensitivity to lip structures, making it unsuitable for precise lip control.

3. Ethical considerations

we recognize that realistic talking face generation may raise ethical concerns regarding potential misuse, such as creating deceptive or malicious deepfake content. To mitigate such risks, all generated videos in our study can be clearly marked as synthetic (Fig. 3), ensuring transparent presentation of results. We strongly advocate that any future application of this technology should comply with ethical stan-

dards and obtain informed consent when involving identifiable individuals.